Available online at www.sciencedirect.com
ScienceDirect
Progress in Natural Science 18 (2008) 1365–1373
Progress in Natural Science
www.elsevier.com/locate/pnsc

A new parameterization scheme for sea surface aerodynamic roughness

Yuping Pan [a,b], Wenyu Sha [c], Shouxian Zhu [c], Sufang Ge [a,*]

[a] Nanjing University of Information Science and Technology, Nanjing 210044, China
[b] Air Force Meteorological Center of the Nanjing Military Region, Nanjing 210018, China
[c] Meteorology College, The PLA University of Information Science and Technology, Nanjing 211101, China

Received 21 February 2008; received in revised form 25 March 2008; accepted 14 May 2008

Abstract

The dimensionless roughness length derived from dimensional analysis bears a relation to wave age, and the dimensionless form of roughness length can be expressed with the relation with a significant wave height. Based on six experiments (HEXMAX, RASEX, BIO steady platform, Lake Ontario data analysis FETCH, CBLAST low wind), we verified that the Charnock parameter, z_{ch}, and dimensionless roughness length, z_0/H_s, are dependent on wave age, u_*/c_p. Moreover, we constructed a new scheme for roughness length, and explored its sensitivity to friction velocity and wave age. Combining the newly developed parameterization scheme (PS07) with COARE (Coupled Ocean-Atmosphere Response Experiment V.3.0) algorithm, we calculated the data from the North Sea Platform experiment in December, 1985, and made an attempt to validate the suitability of the PS07 compared to the other three schemes of COARE. We found that the calculated results based on the PS07 are close to the measurements. We also conducted an experiment in which the PS07 was combined with the nested model of waves coupling in datasets of 3 typhoons that occurred at the Zhanjiang Seaport. The comparison results between the calculated and observed waves around the Naozhou Island indicate that the new parameterization scheme (PS07) has a good applicability.

Keywords: Sea surface roughness; Parameterization scheme; Significant wave height; Wave age; COARE algorithm

1. Introduction

The effects of air–sea interactions on climate and environment are mainly realized through the exchange of momentum, heat and vapor between air and sea [1,2]. Generally, accurate determination of momentum exchange in the interface depends largely on the following two aspects: (1) reasonable description of momentum exchange dependence on atmospheric stability, and (2) precise determination of sea surface aerodynamic roughness. Monin–Obukhov similarity theory has successfully expressed the momentum exchange dependence on atmospheric stability [3,4]. However, how to accurately determine sea surface aerodynamic roughness remains a hot topic in this field [5–11].

Waves are associated with atmospheric motion such that the underlying cause lies in air–sea interactions. The intensity of waves hinges on the acquisition of energy from air movement and has an impact on sea roughness. So, we can attempt to define the energy from air in motion to waves. As a result, in-depth research on sea roughness is helpful for the accurate calculation of air–sea momentum exchange and wave vigor, thus providing information for the reference to modeling research.

The typical parameterization scheme for sea surface roughness is based on the Charnock relationship [12], in which Charnock parameter varies in different experiments. Yelland and Taylor [7] proved that the Charnock parameter could be considered as a linear relation on the condition that wind velocities varied in 10–18 m s^{-1}. More recently, many experimental results indicated that the sea surface roughness is related to wind wave features. Taylor and Yelland [9]

* Corresponding author. Tel.: +86 25 58699761.
E-mail address: sfge001@163.com (S. Ge).

1002-0071/$ - see front matter © 2008 National Natural Science Foundation of China and Chinese Academy of Sciences. Published by Elsevier Limited and Science in China Press. All rights reserved.
doi:10.1016/j.pnsc.2008.05.006

reported that sea surface aerodynamic roughness bears an intimate relation to wave steepness, and they constructed a parameterization scheme for this relation (referred to as TY01 hereinafter). On the other hand, the work of Oost et al. [10] (referred to as O02 thereafter) proved that the sea surface roughness could be considered as functions of wave age and frictional speed. Both the equations (TY01 and O02) are included in the new version of Coupled Ocean-Atmosphere Response Experiment (COARE) algorithm. Considering the importance of aerodynamic roughness to the study of wave development and air–sea interaction, we think it is necessary to improve the precision and applicability of the calculation for sea surface roughness.

2. Dimensional analysis

The roughness length is related to wind stress (U) and sea state (W):

$$U = f(u_*, dir_a, \rho_a, v_a, T_a, g) \tag{1}$$

$$W = g(H_s, T_p, dir_w, h, \rho_w, v_w, T_w, g, z_{0s}) \tag{2}$$

in which u_* stands for friction velocity; dir_a and dir_w stand for wind and wave directions, respectively; ρ_a, v_a and T_a for air density, viscosity and temperature, respectively; H_s stands for the significant wave height; T_p for the peak period; ρ_w, v_w and T_w are the sea water density, viscosity and temperature, respectively; h is the water depth; g is the gravitational acceleration; and z_{0s} is the background roughness.

The sea surface roughness length can be expressed as $z_0 = F(U, W)$. From (1) and (2), we can get

$$z_0 = F(u_*, dir_a, \rho_a, v_a, T_a, g, H_s, T_p, dir_w, h, \rho_w, v_w, T_w, z_{0s}) \tag{3}$$

Then, using ρ_a, u_*, g and H_s as the substitutes, we can change (3) to a dimensionless form, that is

$$\frac{z_0}{H_s} = G\left(\frac{gT_p}{u_*}, \frac{gh}{u_*^2}, \frac{gz_{0s}}{u_*}, \frac{u_*^3}{gv_a}, \frac{u_*^3}{gv_w}, \frac{T_w}{T_a}, \frac{dir_w}{dir_a}, \frac{\rho_w}{\rho_a}\right) \tag{4}$$

Now, the following assumptions are considered:

(i) The dispersion relation $c_p^2 = g/hthkh$ is used to make the gT_p/u in a form relative to phase velocity c_p. Assuming deep-water condition, we can ignore the term gh/u_*^2, and get

$$\frac{gT_p}{u_*} = 2\pi\frac{c_p}{u_*} \tag{5}$$

(ii) Assuming no waves and a completely smooth surface, we can eliminate gz_{0s}/u_*^2.

(iii) Under the assumption that the surface is in a condition of rough turbulence, we can neglect u_*^3/gv_a and u_*^3/gv_w in Eq. (4).

(iv) T_w/T_a represents the effect of sea water and air temperatures on the momentum fluxes at the interface of sea and air. In the condition of neutral stratification, the temperature difference between air and water is very small and could be neglected.

(v) For zero background roughness, directions of wind and wave are much the same, so that the dir_w/dir_a can be eliminated.

(vi) ρ_w/ρ_a is a constant and could be dropped.

When the above assumptions are employed, we can express Eq. (4) as

$$\frac{z_0}{H_s} = \tilde{F}\left(\frac{c_p}{u_*}\right) \tag{6}$$

Eq. (6) indicates that the sea surface roughness length z_0 is related to the significant wave height and wave age. Considering that a conspicuous 3/2 power similarity existed between dimensionless wave height and period, and taking a series of assumptions, Toba concluded that the Charnock parameter is associated with wave age [1]. Here, the dimensionless roughness length is expressed to be in direct relation to the significant wave height due to the following two facts: (i) the sea surface roughness depends not only on roughness element, such as significant wave height, but also on movement factors, such as wave age; (ii) among the elements associated with waves, only the significant wave height can be measured.

Therefore, negligence of the Toba approximate expression could make the description of sea surface roughness even more explicit in its physical implication. And the description is discussed in the context of the aforementioned data.

3. Theoretical development of the sea surface roughness in different experiments

3.1. Experimental data

3.1.1. HEXMAX (humidity exchange over the sea main experiment)

As a part of the HEXOS (humidity exchange over the sea), the HEXMAX experiment was conducted in October and November, 1986. The HEXMAX experiment was conducted on the Meetpost Noordwijk (MPN) platform in the vicinity of the Netherlands coast in the southern North Sea, and the purpose of this experiment is to investigate the dependence of drag coefficient and roughness length on sea state, and to measure the significant wave height and its phase velocity. Sea depth of the research area is 18 m and the fetch length in this area is 175 km, so the HEXMAX results can represent a condition of limited water depth with a long fetch.

3.1.2. RASEX (Riso air–sea exchange) experiment

RASEX was a shallow-water experiment, which was based on two offshore 48-m-high observation towers, and was conducted in the Baltic Sea in the spring and autumn of 1994. We employed the October–November coastward current data of RASEX. All the data were taken in a limited fetch condition, which represents water depth with

3–4 m, offshore fetch length with 2–5 km, and coastward fetch length with 15–25 km.

3.1.3. BIO (Bedford Institute of Oceanography) steady platform experiment

The BIO steady platform experiment was conducted at Sable Island of Nova Scotia, Canada, in 1976–1978. The aim of BIO experiment was to determine the sea surface wind stress by directly measuring the stronger winds, and to understand the variation of drag coefficient with wind velocity, stability and sea state. For nearly half of January, the mean wind velocity at Sable Island exceeded 15 m s^{-1}, so a steady platform was required for withstanding the attacks of 18 m-high wave (peak to valley), strong winds with averaged velocity of 45 m s^{-1} and gust wind factor of 1.25, and sea current velocity of 0.25 m s^{-1}. The sea area in which research was done is 59 m deep, which allows 99% of 10 s-wave to travel at deep-water phase velocity. So, waves in this area are typically deep-water waves. Moreover, under the effect of southerly and easterly winds that originated from the North Atlantic, the wind zone could be regarded as a long fetch. Under the condition of west winds that originated from the coast, the minimum wind fetch was 10 km long.

3.1.4. Research results from Lake Ontario data

Over the Lake Ontario there were two buoy stations where surface meteorological data were plenty. To obtain simultaneous fluxes and wave parameter data, we employed the data from the Lake Ontario by Anctil et al. [13]. The data were taken from four meteorological observation stations, at which water depth was 2, 4, 8 and 12 m during two wind events. The mean wind over 166 steps was about 7 m s^{-1} over about 8 km fetch, while the mean wind over 185 steps was about 14 m s^{-1} over about 300 km fetch.

3.1.5. FETCH (Flux, Etat de la mer, et Télédétection en Condition de Fetch variable) experiment

FETCH experiment was performed in the northern Mediterranean Sea from March 12 to April 15, 1998. The aim of FETCH experiment was to estimate the off-shore turbulent flux, reveal the evolution of waves, and analyze the remote soundings of the air–sea boundary layer. Due to coastward winds that prevailed in northern Mediterranean Sea, long fetch condition predominated in this area. In this study, we made use of the observations from the weather ship named R/V L'Atlante.

3.1.6. CBLAST (the coupled boundary layer air–sea transfer)-low wind experiment

The CBLAST-low wind experiment was the part of the low wind component in the CBLAST experiment. The experiment was performed at the Nantucket Island of Massachusetts, USA, from July 22 to August 27, 2003. The main purpose of this experiment was to explore the boundary layer characteristics under a range of meteorological conditions and to provide *in situ* evidence for assessing mesoscale models. We made use of synchronous meteorological observations from the Air–Sea Interaction Tower (ASIT) around the Martha Vineyard port.

3.2. Establishment of the parameterization scheme

The results from single experiments varied from one condition to another. So, to validate the u_*/c_p dependence on z_0/H_s and z_{ch}, we employed results from the above-mentioned six experiments. Our results are shown in Fig. 1.

Fig. 1a and b indicate that the logarithmic forms of dimensionless roughness length (z_0/H_s) and the Charnock parameter (z_{ch}) are in good linear relation with that of the inverse of u_*/c_p, with their respective correlation coefficients 0.8274 and 0.6313. And their linear regression equations could be expressed as $\ln\frac{z_0}{H_s} = 2.82\ln\left(\frac{u_*}{c_p}\right) - 0.295$ and $\ln z_{ch} = 1.4\ln\left(\frac{u_*}{c_p}\right) - 0.06$, respectively. Considering Zhang's [14] suggestion that sea surface roughness length and the inverse of wave age are in an exponential relation, we present a semi-logarithmic distribution of z_0/H_s and z_{ch} with respect to the inverse of u_*/c_p, as given in Fig. 1c and d, respectively. From Fig. 1c and d, we could see that the point distribution for logarithmic forms of z_0/H_s and z_{ch} relating to u_*/c_p are relatively concentrated, and their linear relations are insignificant, with relatively lower correlation coefficients of 0.7419 and 0.5359, respectively. Obviously, the HEXOS relationship between z_0/H_s (z_{ch}) and u_*/c_p $\left(\left(\frac{z_0}{H_s}, z_{ch}\right) = \alpha(u_*/c_p)^{\beta}\right)$ is superior to their exponential relation. Fig. 1e and f indicate that the point distribution of z_0/H_s and z_{ch} in relation to wave steepness in their logarithmic forms is greatly scattered, particularly in the low-wind portion, with their correlation coefficients of 0.5172 and 0.3837, respectively. From the above comparison results, we can conclude that the linear relation is most significant between the logarithmic forms of z_0/H_s and the inverse of u_*/c_p, with a correlation coefficient of 0.8272.

3.3. Test of the linear regression

The linear regression equation is

$$\ln\frac{z_0}{H_s} = 2.82\ln\left(\frac{u_*}{c_p}\right) - 0.295 \tag{7}$$

The statistical significance test was performed for the regression coefficient and constant term, and the optimality test was performed for predictions (Table 1).

Table 1 shows that the standard errors of the regression coefficient and constant term are 0.0666 and 0.2384, t statistics of which are 42.4189 and 1.2385, and p values are 0 and 0.2159, respectively. The t test indicates that the regression coefficient and constant term are statistically significant within their confidence intervals. The coefficient of determination and its modification are 0.6846 and 0.6842, indicating a relative better fitness of samples by the regression model. In Table 1, for variance estimation, Model

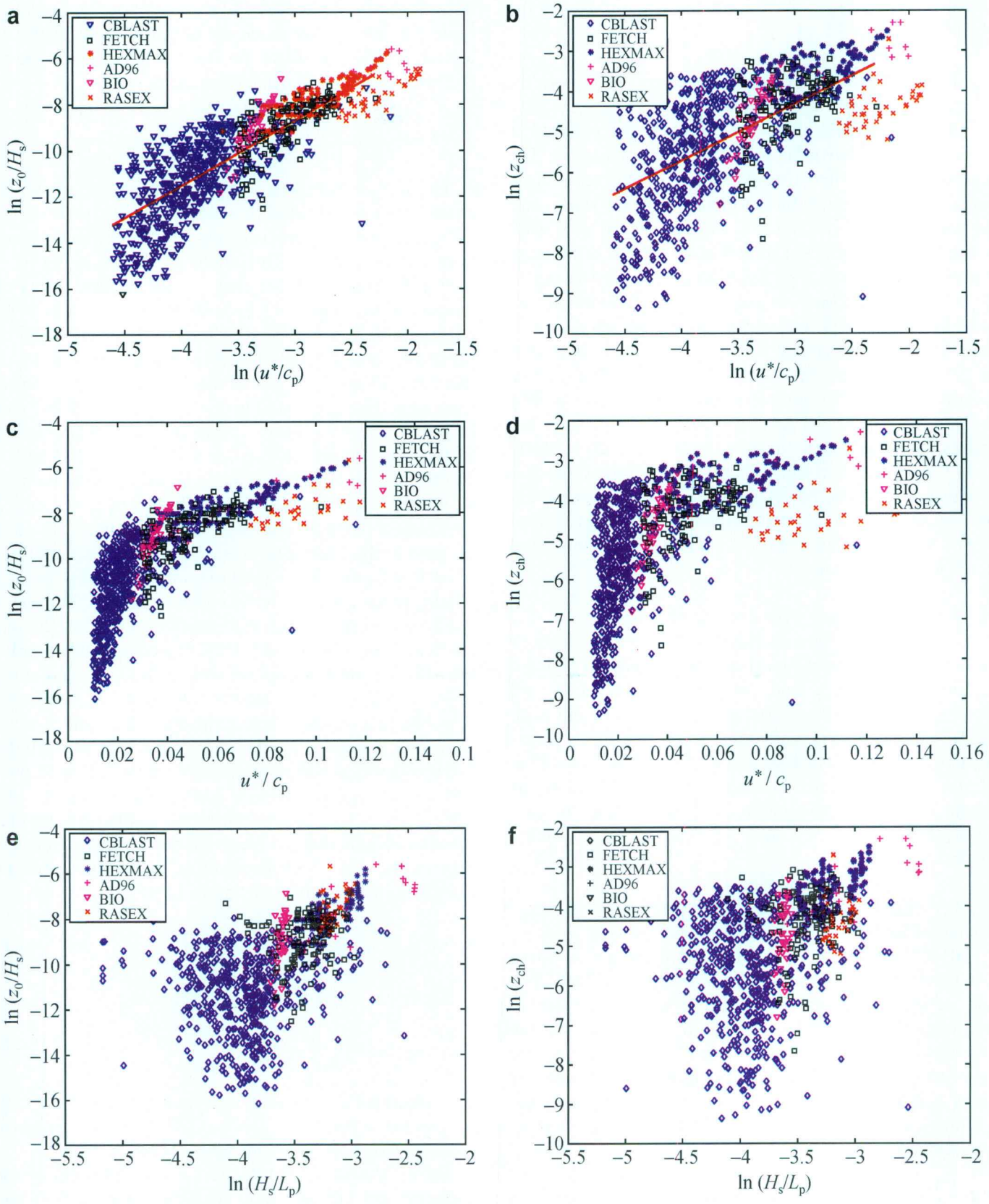

Fig. 1. Dimensionless roughness length, z_0/H_s, and Charnock parameter changing with the inverse of wave age (a–d) and steepness (e and f).

stands for the sum of squared regression values (2557.82); Error for the sum of squared residuals (1178.44); and Total for the sum of squared differences between observations and fittings (3736.26). F value is high enough to reach 1799.36, rejecting the zero hypothesis for events of small probability, and indicating a high linear relation between the logarithmic forms of z_0/H_s and the inverse of u_*/c_p at 0 significance level.

Table 1
Parameters of the linear regression

Parameter		Estimate	SE	t test	p value
1		0.29522	0.238359	1.2385	0.21587
x		2.82445	0.066585	42.4189	0
	df	Sum of sq.	Mean sq.	F ratio	
Model	1	2557.82	2557.82	1799.36	0
Error	829	1178.44	1.4215		
Total	830	3736.26			

R^2: 0.684595, adjusted R^2: 0.684214, estimated variance: 1.42152.

4. Sensitivity experiment

4.1. Sensitivity of sea surface roughness length to friction velocity

From the roughness length $z_0 = \frac{10}{\exp(ku_{10}/u_*)}$, we know that z_0 is related to the von Karman constant k, the wind speed u_{10} and the frictional velocity u_*. Following Johnson et al. [15], we assume that the errors of k, u_{10} and u_* can be expressed in the form of $\Delta k/k$, $\Delta u_{10}/u_{10}$. and $\Delta u_*/u_*$. So, the error of z_0 has the form

$$\frac{\Delta z_0}{z_0} + 1 = \exp\left\{\frac{-k/\sqrt{C_D}}{(1+\Delta u_*/u_*)}\left[\frac{\Delta u_{10}}{u_{10}} + \frac{\Delta k}{k} + \frac{\Delta k}{k}\frac{\Delta u_{10}}{u_{10}}\frac{\Delta u_*}{u_*}\right]\right\} \tag{8}$$

Considering the fact that k is taken as 0.4 and u_{10} also has a smaller error (generally <2%), we think the error of z_0 has mainly originated from u_*. If we take C_D as 0.0012, which is the average value obtained from the experimental data, and assume ±10% error in u_*, the error of $\Delta z_0/z_0$ will reach 185%. If we assume ±5% error in u_*, the error of $\Delta z_0/z_0$ will be 73%. Obviously, the roughness length is highly sensitive to friction velocity. As a result, the accuracy for a calculated velocity must be fairly high, otherwise a small error in u_* would lead to a greater error in z_0.

4.2. Sensitivity of roughness length to wave age

Error in wave age could be taken as

$$\frac{\Delta(c_p/u_*)}{c_p/u_*} = \frac{\Delta c_p/c_p - \Delta u_*/u_*}{1+\Delta u_*/u_*} \tag{9}$$

If we neglect the error of c_p and assume ±10% error in u_*, the errors in wave age will be ranged from −9% to 11%. From (9), we can see that the error of wave age is smaller than those of wave phase speed and friction velocity. Consequently, roughness length and drag coefficient are the function of wave age. So, it is possible to reduce the errors of roughness length and drag coefficient in the calculation.

From the equations for roughness length and wave age, we have

$$\frac{\Delta z_0}{z_0} + 1\left[1 + \frac{\Delta(c_p/u_*)}{c_p/u_*}\right]^{-2.82}\left(1 + \frac{\Delta H_s}{H_s}\right) \tag{10}$$

If we just consider the effect of wave age on roughness length and assume ±10% error in u_*, the errors of wave age and roughness length will range from −9% to 11% and from −25% to 30%, respectively. For ±5% error in u_*, the corresponding errors of wave age and roughness length will range from −4.8% to 5.3% and from −13.6% to 14.8%, respectively. In the case of the same error, the error of roughness length is much smaller than that of friction velocity.

5. Test of sea surface roughness

5.1. Materials and method

In order to test the applicability of the newly developed scheme for sea surface roughness, we make use of the data which was obtained from the FPN platform at North Sea during the first two weeks of December 1985. The FPN platform is 65 km to the southwest of Westerland (Sylt) in German Bight, and water depth in this area is 30 m. The main purpose of FPN experiment was to assess wind stress and backscattering features of radar scatter under the condition in which the wind velocity varied greatly [16]. Of the 116 time-level observations, prevailing winds were southerly and SW from December 4 to December 6 at 06:00 UTC, maximizing at 16.22 m s^{-1} at 04:00 UTC, December 6, followed by wind veering to NW, with wind velocity further intensifying to 24.43 m s^{-1}. The wind began to abate at 17:00 UTC, December 6, minimizing at 21:00 UTC, with wind veering to SSW. Winter temperature was rather low, with relatively small temperature difference between sea and air. As a storm approached, atmospheric temperature dropped sharply, leading to positive-valued difference between sea and air. Significant wave height increased with amplified winds, reaching a maximum of 7.08 m at 10:00 UTC, December 6.

5.2. COARE algorithm

COARE algorithm is based on Monin–Obukhov similarity theory, and is a further breakthrough compared with the algorithm made by Liu et al. [17] The latest edition is V3.0 in which wave information is included [5].

COARE provides three parameterization schemes for aerodynamic roughness length: YT96, TY01 and O02.

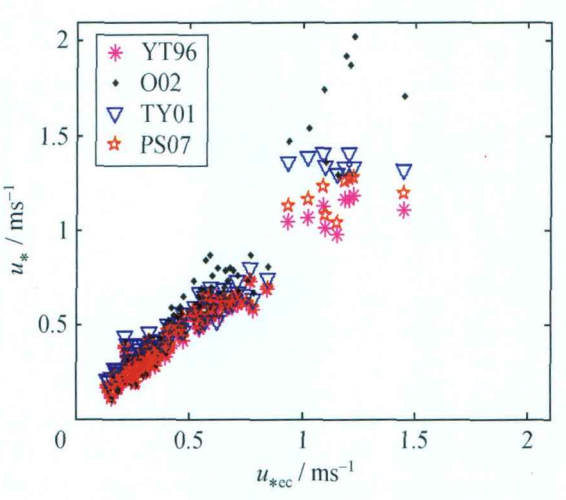

Fig. 2. The scatter plot of calculated and measured frictional velocities.

Among the three schemes, only YT96 makes use of the Charnock relation, the other two are associated with wave conditions. For the detailed parameterization schemes, the reader could refer to Ref. [18].

5.3. Data analysis

We calculated the frictional velocity, drag coefficient and momentum flux for the North Sea FPN platform experiment by introducing the new scheme (PS07) into the COARE algorithm. In order to test the suitability of PS07, we compared the results with the measurements of the eddy correlation method and the calculation results obtained by using COARE algorithm (TY01, YT96 and O02). Fig. 2 shows the scattered point distributions of calculated and measured frictional velocities. The calculated linear regression coefficients are as follows: $u_{*_{ed}} = 0.899u_{*_{TY}}, u_{*_{ed}} = 1.045u_{*_{YT}}, u_{*_{ed}} = 0.784u_{*_0}$ and $u_{*_{ed}} = 1.007u_{*_{PS}}$. These results indicate that the TY01 and O02 methods overestimate frictional velocity; YT96 underestimates frictional velocity; while PS07 gives findings closest to the observations. On the other hand, normalized standard errors of different methods (estimated from $\sqrt{\frac{1}{n}\sum_{i=1}^{n}(A_i - B_i)^2}$, with A_i as the estimated and B_i as the true value) and root-mean-square (rms) errors also indicate that the PS07 calculations are the closest to the observations (Table 2).

Table 2
Normalized standard errors estimate (NSEE) and rms errors of u_*, C_D and τ from the four schemes

	u_* (m s^{-1})		C_D (10^3)		τ (N m^2)	
	NSEE	rms	NSEE	rms	NSEE	rms
YT96	0.1219	0.0623	0.2414	0.384	0.2432	0.1084
TY01	0.1820	0.0931	0.3764	0.599	0.4032	0.1797
O02	0.3350	0.1713	0.6060	0.965	1.0374	0.4623
PS07	0.1188	0.0607	0.2407	0.380	0.2310	0.1029

6. Application of PS07 to the nested model of wind-waves coupling

In order to validate the applicability of PS07 scheme, we made use of it in our self-developed nested model of wind-waves coupling. In the validating research, we calculated waves around the Naozhou Island in the context of the three datasets of typhoons recorded at the Zhanjiang Seaport, and compared the calculated results with *in situ* measurements.

6.1. Brief description of the nested model

The nested model of wind-waves coupling consists of the tropical cyclone wind field, pressure field model and simulating waves nearshore (SWAN) model.

6.1.1. Pressure and wind field model for the tropical cyclone

For the tropical cyclone, pressure and wind fields were calculated by using the self-developed asymmetric pressure model for sea surface pressures [11]. The sea surface winds were calculated based on the principle of gradient winds. The outer-zone winds of the cyclone were offered by NCAR reanalysis data or numerical products, and the winds were also assimilated by single-station observations on a synchronous basis. The initial field that originated from the model winds, corrected on the basis of actual observations, led to an accurate and rational wind field for an actual typhoon.

6.1.2. SWAN model

The wave model employed in the nested model is the third-generation SWAN model, which includes sufficient physical processes with wave growth being described both linearly and exponentially. The exponential growth is depicted only by the Komen expression [19], and the roughness is offered by PS07. For energy dissipation, the mainly considered factors are white cap effect, bottom friction and depth-induced breaks.

6.2. Computational domain, boundary and initial conditions

Fig. 3a and b depict a fanned self-adaptive mesh for the South China Sea (SCS) and a self-adaptive mesh for the Zhanjiang Seaport, respectively. The large-scale mesh in Fig. 3a covered the whole SCS. The grid spacing near the seaport is on the order of 5 km, and the grid length increases up to 80 km far away from the seaport. This mesh design can guarantee computational domain large enough to allow errors in handling at the open boundary. The errors may affect the seaport which is ignorable to a greater degree, and thus reduce the processing difficulty at such a boundary. Meanwhile, a high resolution near the seaport is reached for computational accuracy in the context of a small number of grids for calculation. The grid size at the open boundary is roughly equivalent to that of the SCS

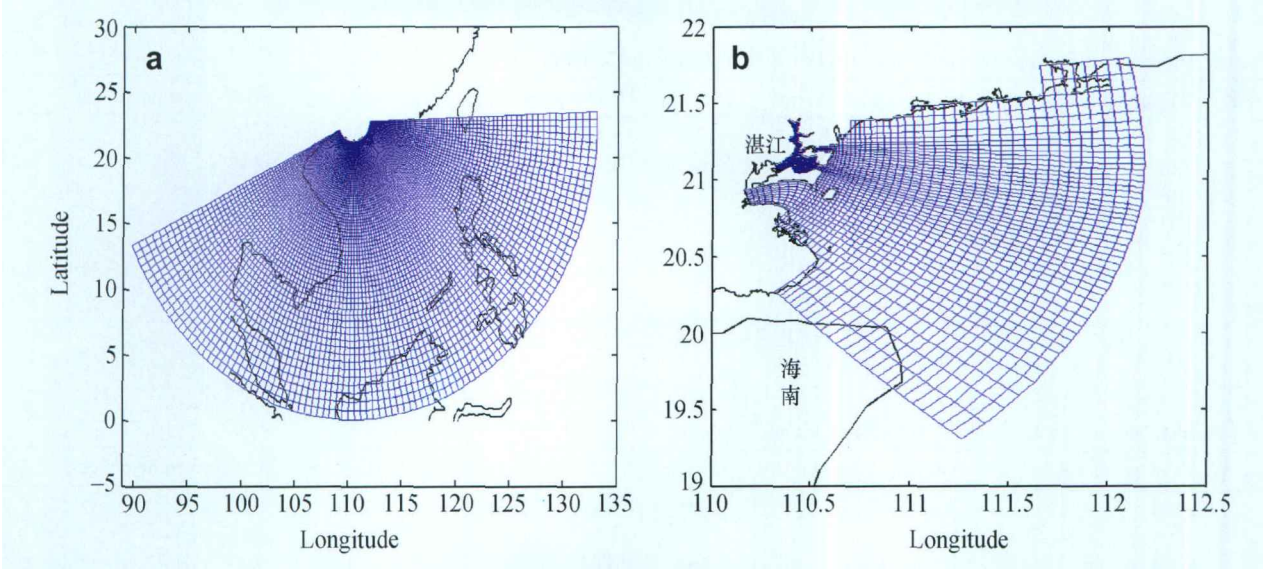

Fig. 3. Self-adaptive mesh over the South China Sea and the Zhanjiang Seaport. (a) The fanned self-adaptive mesh over the South China Sea; (b) the self-adaptive mesh for the Zhanjiang Seaport, with latitudes (longitudes) given on the ordinate (abscissa).

fanned self-adaptive mesh, so it is easy to nest the two domains.

For open boundary condition, the large domain (Fig. 3a) regards the SCS as a closed region and the open boundary consists of changes in water level simulated in the large domain. For initial condition, apart from the open boundary, zero initial condition was put for the computational domain, with integration starting from the rest.

6.3. Validation of wave simulation

Data of tropical cyclones 7818, 8208 and 9713 were taken to test our simulations. The paths of the cyclones are not shown. Because of the absence of wave observing sites in the Zhanjiang Seaport, wave measurements from the oceanic hydrological station on the Naozhou Island were taken for comparison with the modelings. The observation was made 4 times a day (08:00, 11:00, 14:00 and 17:00 BST). Due to the fact that wave observation is greatly subject to oceanic and meteorological conditions, lack of observation occurs frequently and causes discontinuity of data. As a result, when there is a maximum rise in water level, no measurement is available. To effectively test the waves, we made use of the wave heights to calculate the relative error in stimulations and measurements as the cyclone began to significantly affect the observing station.

Tables 3–5 present the wave height observations made around the Naozhou Island under the effect of the given tropical cyclones, in comparison with the predictions from YT96, O02 and PS07, respectively. Due to significant errors from TY01, we do not discuss it here. Tables 3–5 indicate that the significant wave height calculated by using PS07 is the closest to the observation, and its mean errors are the minimum. As to O02, its calculation results were obviously overestimated. Since no wind effects of sea surface condition were taken into account, the H_s calculated by using YT96 was maximum, resulting in the largest mean errors among the three schemes. Based on the three cases of tropical cyclones over a rough sea, we found that the values of Hs were between 0.6 and 3.8 m, which were the closest to the results calculated by using PS07.

Table 3
Predictions vs. observations for the cyclone 7818 which lasted from September 24 to October 4 around the Naozhou Island

Time (day/h)	Observed height (m)	O02-given height (m)	Dif. (m)	YT96-given height (m)	Dif. (m)	PS07-given height (m)	Dif. (m)
30:08	2.9	2.62	−0.88	2.63	−0.87	2.61	−0.9
30:11	2.7	2.73	−0.77	2.74	−0.76	2.67	−0.81
30:14	2.1	2.76	0.26	2.77	0.27	2.71	0.21
30:17	1.8	2.85	0.45	2.85	0.45	2.80	0.39
01:08	1.9	3.83	1.73	3.90	1.8	3.53	1.57
01:11	2.5	4.19	1.19	4.28	1.28	3.71	0.94
01:14	3.3	4.49	−0.01	4.61	0.11	3.93	−0.31
02:08	3.8	4.91	0.61	5.09	0.79	4.01	0.04
02:11	3.5	4.76	0.66	4.95	0.85	3.86	0.09
02:14	2.6	4.08	0.88	4.25	1.05	3.33	0.42
Mean error		0.744		0.823		0.568	

Dif., difference.

Table 4
Predictions vs. observations for the cyclone 8208 which lasted from July 9 to 18, 1982

Time(day/h)	Observed height (m)	O02-given height (m)	Dif. (m)	YT96-given height (m)	Dif. (m)	PS07-given height (m)	Dif. (m)
16:14	0.6	0.22	0.38	0.21	0.39	0.15	0.45
16:17	0.6	0.32	0.28	0.32	0.28	0.34	0.26
17:08	1.8	2.54	0.74	2.54	0.74	2.46	0.66
17:11	2.2	2.94	0.74	3.00	0.8	2.64	0.44
17:14	2.4	2.75	0.35	2.82	0.42	2.40	0
17:17	2.2	2.58	0.38	2.62	0.42	2.22	0.02
Mean error		0.478		0.508		0.305	

Table 5
Predictions vs. observations for the cyclone 9713 which lasted from August 12 to 21, 1997

Time (day/h)	Observed height (m)	O02-given height (m)	Dif. (m)	YT96-given height (m)	Dif. (m)	PS07-given height (m)	Dif. (m)
21:14	1.3	0.41	0.89	0.41	0.89	0.33	0.97
21:17	1.1	0.85	0.25	0.85	0.25	0.62	0.48
22:08	3.4	4.66	1.26	4.83	1.43	3.83	0.43
22:11	3.8	4.65	0.85	4.82	1.02	3.89	0.09
22:17	2.4	4.83	2.43	5.03	2.63	3.52	1.12
23:08	1.7	1.01	0.69	1.00	0.7	1.03	0.67
23:11	1.4	0.96	0.44	0.97	0.43	0.99	0.41
Mean error		0.973		1.050		0.596	

7. Conclusions

The dimensionless roughness length (z_0/H_s) derived from the dimensional analysis is related to wave age (u_*/c_p). Based on the data of the six experiments performed under different conditions, we validated the dependence of z_{ch} and z_0/H_s upon u_*/c_p, and established the regression model of z_0/H_s. The main conclusions could be summarized as follows:

(i) Based on the research of z_0/H_s sensitivity to frictional velocity and wave age, we found that z_0/H_s is highly sensitive to the frictional velocity, z_0/H_s is the function of u_*/c_p, and the related errors could be further reduced in the calculation.

(ii) With the newly developed roughness scheme PS07 introduced into the COARE (V.3.0) algorithm, we employed the data of the 1985 North Sea Platform experiment to test the suitability of the sea surface roughness length parameterization. Our research indicates that O02 and TY01 overestimate frictional velocity, YT96 underestimates frictional velocity and PS07 gives the results closest to *in situ* measurements.

(iii) Using the PS07 in the nested model of waves coupling with 3-typhoon data from the Zhanjiang Seaport, we compared the calculated wave height with the measured wave height around the Naozhou Island, and discovered that our newly developed scheme PS07 has a higher suitability.

Acknowledgement

This work was supported by National Natural Science Foundation of China (Grant No. 40775016).

References

[1] Toba Y, Ebuchi N. Sea-surface roughness fluctuating in concert with wind and waves. J Oceanogr Soc Japan 1991;47(3):63–79.
[2] Dickinson RE, Hendersin-Sellers A, Rosenzweig C, et al. Evapotranspiration models with canopy resistance for use in climate models, a review. Agric For Meteorol 1991;54(4):373–88.
[3] Zhou MY, Li SM, Qian FL, et al. Numerical simulation of energy budget with its variation over China landmass and its offshore belts. J Geophys 2000;245(3):319–29, [in Chinese].
[4] Launiainen J. Derivation of the relationship between the Obukhov stability parameter and the bulk Richardson number for flux-profile studies. Boundary-Layer Meteorol 1995;76(2):165–79.
[5] Fairall CW, Bradley EF, Rogers DP, et al. Bulk parameterization of air–sea fluxes for TOGA COARE. J Geophys Res 1996;101(C2):3747–64.
[6] Donelan M, Dobson FW, Smith SD, et al. On the dependence of sea surface roughness on wave development. J Phys Oceanogr 1993;23(9):2143–9.
[7] Yelland M, Taylor PK. Wind stress measurements from the open ocean. J Phys Oceanogr 1996;26(4):541–58.
[8] Zeng X. Comparison of bulk aerodynamic algorithms for the computation of sea surface fluxes using the TOGA COARE and TAO data. J Clim 1998;11(10):2628–44.
[9] Taylor PK, Yelland MJ. The dependence of sea surface roughness on the height and steepness of the waves. J Phys Oceanogr 2001;31(2):572–90.
[10] Oost WA, Komen GJ, Jacobs CMJ, et al. New evidence for a relation between wind stress and wave age from measurements during ASGAMAGE. Boundary-Layer Meteorol 2002;103(3):409–38.
[11] Sha WY, Yang ZZ, Feng M, et al. Numerical prediction of storm surge and wave. Beijing: Oceanographic Press; 2004, [in Chinese].
[12] Charnock H. Wind stress on water surface. Quart J Roy Meteorol Soc 1955;81(350):639–40.
[13] Anctil F, Donelan MA. Air–water momentum flux observations over shoaling waves. J Phys Oceanogr 1996;26(7):1344–53.
[14] Zhang ZF, Li JC. Effects of wave development on sea surface drag coefficient. J Chin Sci A 1998;28(1):53–61, [in Chinese].
[15] Johnson HK, Hoejstrup J, Vested HJ, et al. Dependence of sea surface roughness on wind waves. J Phys Oceanogr 1998;28(9):1702–16.

[16] Geernaert GL, Larsen SE, Hansen F. Measurements of the wind stress, heat flux and turbulence intensity during storm conditions over the North Sea. J Geophys Res 1987;92(C12):13127–39.

[17] Liu WT, Katsaros KB, Businger JA. Bulk parameterization of the air–sea exchange of heat and water vapor including the molecular constraints at the interface. J Atmos Sci 1979;36(9):1722–35.

[18] Sha WY, Pan YP. COARE algorithm tested four new-edition sea surface aerodynamic roughness schemes. Proc Natl Acad Sci USA 2004;14(2):196–200, [in Chinese].

[19] Komen GJ, Hasselmann S, Hasselmann K. On the existence of a fully developed wind-sea spectrum. J Phys Oceanogr 1984;14(8):1271–85.